



Investigation of the factors affecting acid blue 256 adsorption from aqueous solutions onto red pine sawdust: equilibrium, kinetics, process design, and spectroscopic analysis

Mustafa Can

Vocational School of Arifiye, Sakarya University, 54580 Sakarya, Turkey,
Tel. +0264 295 60 41, +0505 253 2100; Fax: +0264 295 59 50; email: mstfacan@gmail.com

Received 2 June 2014; Accepted 29 December 2014

ABSTRACT

Acid Blue 256 (AB256) dye was selected as the model. Textile effluents and linear and nonlinear regression procedures have been applied to the Langmuir, Freundlich, Tempkin, Dubinin–Radushkevich, and Redlich–Peterson isotherms for adsorption of the dye onto red pine (*Pinus resinosa*) sawdust. The effects of parameters were investigated and interaction was characterized by Fourier transform infrared (FTIR) spectroscopy and SEM/EDAX. Five isotherms were used, and the nonlinear method of the Langmuir isotherm equation was found to provide the closest fit to the equilibrium data. The monolayer adsorption capacity is 54.16 mg/g for AB256. The optimum conditions were found to be: adsorbent size 75–90 μm , initial pH 2, stirring rate 600 rpm, initial dye concentration 200 mg/l, biosorbent dose 1 g and temperature 25°C. All thermodynamic parameters suggested that AB256 adsorption onto red pine sawdust was a spontaneous, physisorption, and exothermic process. Kinetics was analyzed by four different kinetic equations using nonlinear regression analysis. The pseudo-second-order equation provided the best fit with experimental data.

Keywords: Acid Blue 256; Acid dye; Sawdust; Nonlinear regression; Adsorption

1. Introduction

Water demand has increased tremendously resulting in the generation of large amounts of wastewater containing a number of “pollutants” [1]. Because dye is a visible pollutant, the presence of even very small amounts of this molecule is undesirable due to its high visibility. This also makes it the most important factor for removal in industrial wastewater. Some strong dyes containing textile effluents require the employment of a wide range of processes for color removal. These processes involve adsorption on inorganic or organic matrices, decolorization by

photocatalysis and/or by oxidation processes, microbiological or enzymatic decomposition, and others [2].

Chemical and physical methods include the adsorption process, which is one of the more effective methods used to remove dyes from aqueous solutions. In recent years, attention has been directed toward a number of natural solid materials that are able to remove pollutants from contaminated water at low cost [3]. Adsorbent cost is an important factor and present efficiencies and cost estimates for various commercial activated carbons are reported along with the cost of some adsorbents. According to these, bagasse

fly ash, peat, sphagnum moss peat, fuller's earth, BF slag, bentonite, zeolite manganese oxide, and carbonaceous adsorbent are materials costing less than US \$0.01/kg, making them useful materials in terms of cost compared to commercial activated carbons that normally cost more than US\$1.50/kg [4]. As indicated by these figures, red pine sawdust should be used as a low-cost adsorbent.

Classification by application is the principal system adopted by the Color Index (CI). The textile industry uses approximately 10,000 different dyes and pigments [5]. The chemical structure of Acid Blue 256 dye has been disguised by the manufacturer. Several studies on the removal of metal complex dyes are found in the literature [6–10] describing agricultural biosorbents used for the removal of dyes from aqueous solutions [9–14]. Among the untreated materials investigated, many agricultural residues, such as wheat straw, rice husk, corncobs, and wood chips have been used successfully to adsorb individual dyes and dye mixtures in textile effluent. However, only limited numbers of studies have been carried out with sawdust [15,16]. Sawdust is a waste byproduct of the timber industry that does not noticeably swell in water or decompose upon prolonged contact with water. Despite its interesting adsorption capacities, to the best of our knowledge no tests have been done with red pine sawdust covering equilibrium, kinetics and the one-step batch adsorber design of the metal complex dye adsorption.

In this study, red pine sawdust (*Pinus resinosa*) was used as the biosorbent for the removal of metal complex dyes, because *P. resinosa* is found abundantly in Turkey. The main aim of this study is to understand its process. For this purpose, we investigated the effects of particle size and dose of sawdust, pH, contact time, and initial dye concentration on the adsorption of metal complex dyes onto red pine sawdust. The Langmuir, Freundlich, Temkin, Dubinin–Radushkevich (D–R), and Redlich–Peterson (R–P) isotherms were used to match the equilibrium data. This paper also presents the thermodynamic parameters related to the adsorption of MG such as Gibbs free energy change (ΔG°); enthalpy change (ΔH°); and entropy change (ΔS°) that have been calculated and discussed. Furthermore, the kinetics involved in the sorption process was evaluated at different initial acid blue 256 concentrations using a pseudo-first- and second-order equation, intraparticle diffusion equation, and the Elovich equations. Kinetic parameters and Langmuir constants of experimental data were calculated with the nonlinear regression method using Microsoft Excel's Solver Extension software program. Chi-square test was used to evaluate

the models which had the best fit with experimental data. In recent years, a number of low-cost, commercially available adsorbents have been tested for metal complex dye removal, but sawdust has been used sparingly for the removal of metal complex dyes. However, only two papers [13] and [3] have appeared regarding the design of adsorption treatment systems. This paper also develops a single-stage batch adsorber design model. A design analysis method has been developed to predict the required amount of sawdust at various volumes of effluent treated for different percentages of dye removal.

2. Experimental procedures

2.1. Materials

Turkish red pine sawdust was collected from a local lumber mill. It was acid-hydrolyzed to removing sugars from the wood (0.5 M HCl). Then it was washed with distilled water to remove the surface-adhered particles and water soluble materials, and finally dried at 353 K overnight in the drying incubator. After drying, the sawdust was sieved to obtain ≤ 53 , 53–75, 75–90, 90–150, and 150–500 μm size fractions using ASTM standard sieves. Then it was used directly as adsorbent.

AB256 was obtained from Setas Kimya (Istanbul, Turkey). All chemicals were of analytical grade and purchased from Merck (Darmstadt, Germany) or Fluka (Neu-Ulm, Germany), unless otherwise stated.

2.2. Batch adsorption studies

The effect of particle size changing from ≤ 53 , 53–75, 75–90, 90–150, to 150–500 μm range was studied using two dyes on red pine sawdust particles. To study the influence of pH on the adsorption capacity of pine sawdust for AB256 dye, experiments were performed using different initial solution pH values, changing from 2 to 11. Solutions pH was adjusted with dilute HCl and NaOH solutions with the aid of a pH meter. At the same time, the effect of mixing speed was investigated by changing the speed between 200 and 600 rpm. In order to investigate the effect of adsorbent dosage on the adsorption capacity of red pine sawdust for dyes, experiments were performed between 0.5 and 3 g adsorbent. To determine the thermodynamic parameters of adsorption, experiments were performed at different temperatures between 298 and 353 \pm 2 K. Dye solutions (1,000 ml) of 100 mg/L initial concentration were treated with 1 g of the adsorbent on a mechanical stirrer for 3 h, followed by centrifugation. About 5 mL of samples

were centrifuged and the solutions were filtered through a filter paper to avoid any solid particles in the aqueous phase. The supernatant solution was analyzed for residual dye concentration using an ultraviolet–visible spectrophotometer (Shimadzu UV-150-02), and all dye concentrations were measured at the wavelength corresponding to maximum absorbance.

A volume of the AB256 dye solutions with concentrations ranging from 25 to 300 mg/L were placed in 1 L conical flasks. Optimum working pH was adjusted before biosorbent was added. An accurately weighed amount (1 g) of Turkish red pine tree sawdust was added to the solutions. The conical flasks were then agitated at a constant speed of 200 rpm in a water bath set at 298 ± 2 K. Total contact time was selected as 180 min.

Once maximum absorbance, λ_{max} , was determined, these values were used for analyzing. The supernatant solution was analyzed for residual dye concentration using an ultraviolet–visible (UV–vis) spectrophotometer (Shimadzu UV-150-02) at 584 nm for the AB256 dye. The samples were withdrawn from the stirrer at predetermined time intervals and the dye solution was separated from the adsorbent by centrifugation at 5,000 rpm for 15 min.

The point of zero charge of Turkish red pine tree sawdust was determined in order to understand the adsorption mechanism. The pH drift method was used to measure the pH at the potential of zero charge (pH_{zpc}) of Turkish red pine tree sawdust. The pH of a solution of 0.01 M potassium nitrate (KNO_3) was adjusted to between pH 2 and 12. Adsorbent (0.10 g) was added to 20 ml of the solution. After the pH had stabilized (typically after 24 h), the final pH was recorded. The graphs of final vs. initial pH were used

to determine the points at which initial pH and final pH values were equal. This was taken as the point of zero charge.

2.3. Instrumentation

The field emission scanning electron microscope (FE-SEM) used in the study was a Quanta FEG 450 field emission scanning electron microscopy. The SEM and EDAX tests were carried out on samples operating at 10 and 20 kV, respectively, which were Au coated. The magnifications were from $\times 100$ to $\times 100,000$.

FTIR spectra were obtained using a spectroscope (PerkinElmer Spectrum Two Spectrometer). Samples were analyzed in attenuated total reflectance (ATR) mode using ceramic light source, KBr/Ge beam splitter, and deuterated l-alanine triglycine sulfate (DLATGS) detector. The sampling technique used was diffuse reflectance. The powder samples were scanned for wavenumber $600\text{--}4,000\text{ cm}^{-1}$.

2.4. Adsorption isotherms

To simulate the adsorption isotherm, five commonly used models, the Langmuir, Freundlich, Temkin, Dubinin–Radushkevich, and Redlich–Peterson, were selected to explain dye–pine sawdust interactions. These isotherms and their linear forms can be seen in Table 1.

The Langmuir equation initially derived from kinetic studies is based on the assumption that on the adsorbent surface, there is a definite and energetically equivalent number of adsorption sites. The bonding to

Table 1
Adsorption isotherms and its linear forms

	Isotherm	Linear Form	X & Y	Slope & cut-off point
Langmuir linear [17,18]	$q_e = \frac{K_L C_e}{1 + a_L C_e}$	$\frac{C_e}{q_e} = \frac{1}{K_L} + \frac{a_L C_e}{K_L}$	$x = C_e$ $y = C_e/q_e$	$\tan \alpha = \frac{a_L}{K_L}$ cutoff = $\frac{1}{K_L}$
Lineweaver–Burk linear [19]		$\frac{1}{q_e} = \frac{1}{K_L} \frac{1}{C_e} + \frac{a_L}{K_L}$	$x = 1/C_e$ $y = 1/q_e$	$\tan \alpha = \frac{1}{K_L}$ cutoff = $\frac{a_L}{K_L}$
Freundlich [20]	$q_e = K_f C_e^{1/n}$	$\log q_e = -\log K_f + \frac{1}{n} \log C_e$	$x = \log C_e$ $y = \log q_e$	$\tan \alpha = \frac{1}{n}$ cutoff = $-\log K_f$
Temkin [21]	$q_e = \frac{RT}{b} \ln(AC_e), RT/b = B$	$q_e = B \ln A + B \ln C_e$	$x = \ln C_e$ $y = q_e$	$\tan \alpha = B$ cutoff = $B \ln A$
(D–R) [22,23]	$q_e = q_m e^{-\beta \varepsilon^2}, \varepsilon = RT(1 + \frac{1}{C_e})$	$\ln q_e = \ln q_m - \beta \varepsilon^2$	$x = \varepsilon^2$ $y = \ln q_e$	$\tan \alpha = \beta$ cutoff = q_m
(R–P) [24]	$q_e = \frac{AC_e}{1 + BC_e^g}$	$\ln\left(\frac{AC_e}{q_e} - 1\right) = g \ln(C_e) + \ln(B)$	–	–

the adsorption sites can be either chemical or physical, but it must be sufficiently strong to prevent displacement of adsorbed molecules along the surface. Thus, localized adsorption was assumed as being distinct from nonlocalized adsorption, where the adsorbed molecules can move along the surface. Because the bulk phase is constituted by a perfect gas, lateral interactions among the adsorbate molecules were neglected. A monolayer surface phase is thus formed on the energetically homogeneous surface of the adsorbent. Langmuir introduced a clear concept of the monomolecular adsorption on energetically homogeneous surfaces for the first time [17,18].

Although there have been five different linear forms of Langmuir isotherm equation named Langmuir [17], Competitive Langmuir [25], Lineweaver–Burk [19], Eadie–Hofstee [21–23], Scatchard [26–29], and log-log [28,30], the two most commonly used forms are given in Table 1. Lineweaver–Burk linear form [19], is very sensitive to errors, especially at the lower left corner of the chart, and is in very good agreement with the experimental data [30,31]. The K_L and a_L are the Langmuir isotherm constants and the K_L/a_L gives the theoretical monolayer saturation capacity, Q_0 .

The essential features of the Langmuir isotherm can be expressed in terms of a dimensionless constant called separation factor (R_L), which is defined by the following equation:

$$R_L = \frac{1}{1 + a_L C_0} \quad (1)$$

where C_0 (mg/L) is the initial dye concentration and a_L (L/mg) is the Langmuir constant related to the energy of adsorption. In this context, the value of R_L indicates the shape of the isotherms to be either unfavorable ($R_L > 1$), linear ($R_L = 1$), favorable ($0 < R_L < 1$), or irreversible ($R_L = 0$) [32,33].

Freundlich isotherm is widely applied in heterogeneous systems especially for organic compounds or highly interactive species on activated carbon and clays. The Freundlich isotherm is an empirical equation employed to describe heterogeneous systems and the equation is shown in Table 1. In this equation, K_f , ($\text{mg}^{1-1/n} \text{L}^{1/n} \text{g}^{-1}$) is the Freundlich constant related to the bonding energy, and n , (g/L) is the heterogeneity factor. The slope ($1/n$) ranging between 0 and 1 is a measure of adsorption intensity or surface heterogeneity, and it becomes more heterogeneous when its value gets closer to zero. A value below unity implies chemisorption process where $1/n$ above one is an indicative of cooperative adsorption [32,34].

This model is the earliest known relationship describing the nonideal reversible multilayer

adsorption with nonuniform distribution of adsorption heat and affinities over the heterogeneous surface. In this perspective, the amount adsorbed is the summation of adsorption on all sites (each having bond energy), with the stronger binding sites being occupied first until adsorption energy is exponentially decreased upon the completion of the adsorption process [35]. Its linearized and nonlinearized equations are listed in Table 1. The Freundlich isotherm is criticized for its limitation of lacking a fundamental thermodynamic basis, which does not approach the Henry's law at vanishing concentrations [36].

By ignoring the extremely low and large value of concentrations, the derivation of the Temkin isotherm assumes that the fall in the heat of sorption is linear rather than logarithmic. Temkin equation is excellent for predicting the gas phase equilibrium. Conversely, complex adsorption systems including the liquid-phase adsorption isotherms are usually not appropriate to be represented [37]. In this equation, A (L/mg) is the equilibrium binding constant corresponding to the maximum binding energy, b (J/mol) is the Temkin isotherm constant, and constant B (dimensionless) is related to the heat of adsorption.

Radushkevich [23] and Dubinin [22] have reported that the characteristic sorption curve is related to the porous structure of the sorbent (Table 1). Where the constant, β , (mmol^2/J^2) is D–R constant related to the mean free energy of sorption per mole of the sorbate, as it is transferred to the surface of the solid from infinite distance in the solution and can be correlated using the following relationship:

$$E = \frac{1}{\sqrt{2\beta}} \quad (2)$$

and q_m , (mmol/g) is denoted as the single layer capacity. In a deeper explanation, E value indicates the mechanism of the adsorption reaction. When $E < 8$ kJ/mol, physical forces may affect the adsorption. If E is $8 < E < 16$ kJ/mol, adsorption is governed by ion exchange mechanism, while for the values of $E > 18$ kJ/mol, adsorption may be dominated by particle diffusion [38]. The model has often successfully fitted high solute activities and the intermediate range of concentrations data, but has unsatisfactory asymptotic properties and does not predict the Henry's law at low pressure [32]. Meanwhile, the parameter ε is known as Polanyi potential and can be correlated as:

$$\varepsilon = RT \left(1 + \frac{1}{C_e} \right) \quad (3)$$

where R , T , and C_e represent the gas constant (8.314 J/mol K), absolute temperature (K), and adsorbate equilibrium concentration (mg/L), respectively.

The Redlich–Peterson isotherm contains three parameters ($A(L/g)$, $B(L/mg^{1-1/A})$, g) and incorporates the features of the Langmuir and Freundlich isotherms [24]. Its equation and linear form can be seen in Table 1. Isotherm unitless constants g is between $0 < g < 1$ values. When $g = 1$, adsorption isotherm fits Langmuir isotherm. If $g = 0$, isotherm is now fully fits Freundlich isotherm [32,39]. Values between this concern isotherm representation. Due to this versatility, it can be applied either in homogeneous or heterogeneous systems.

Hence, because of containing tree constant, it has been suggested that the nonlinear method is a better way to obtain the isotherm parameters. A trial-and-error procedure, which is applicable to computer operation, was used to compare the best fit of the three isotherms using an optimization routine to minimize the coefficient of determination sum of the squares of the errors, between the experimental data and isotherms in the solver add-in with Microsoft's Excel [40]. In addition, the Redlich–Peterson isotherm equation can be resolved by the linear regression method by making it linear form.

2.5. Adsorption kinetics

In the industrial usage of adsorbents, the time dependence of adsorption on solid surfaces is described as adsorption kinetics. To examine the mechanism of adsorption process such as mass transfer and chemical reaction, a suitable kinetic model is needed to analyze the rate data. Many models such as homogeneous surface diffusion model, pore diffusion model, and heterogeneous diffusion model (also known as pore and diffusion model) have been extensively applied in batch reactors to describe the transport of adsorbates inside the adsorbent particles [41]; however, the mathematical complexity of these models makes them rather inconvenient for practical use. The

large number and array of different functional groups on the activated carbon surfaces (e.g. carboxylic, carbonyl, hydroxyl, ether, quinone, lactone, and anhydride) indicate that there are many types of adsorbent–solute interactions. Any kinetic or mass transfer representation is likely to be global. From a system design viewpoint, a lumped analysis of kinetic data is sufficient for practical operation.

Five commonly used models, pseudo- first- and second-order equation, intraparticle diffusion equation, and the Elovich equation were applied for dye–red pine sawdust interactions. These isotherms can be seen in Table 2.

In 1898, Lagergren expressed the pseudo-first-order rate equation for liquid–solid adsorption systems based on solid capacity [42]. Later, this equation became known as the pseudo-first-order equation.

In recent years, a second-order kinetic equation has described sorption, which included chemisorption and provided a different idea to the second-order equation called a pseudo-second-order rate expression [43]. The process can be described by a pseudo-second order model based on the assumption that the rate limiting step may be chemical sorption or chemisorption between sorbent and sorbate. The parameter that influences the kinetics of the sorption reaction was the sorption equilibrium capacity, q_e , which is a function of initial dye concentrations, red pine sawdust dose, and nature of the dyes. The pseudo-second-order equation has the following advantages: it does not have the problem of assigning an effective sorption capacity; the sorption capacity, rate constant of pseudo-second-order, and the initial sorption rate can all be determined from the equation without knowing any parameter beforehand [44].

The other method of investigating adsorption–desorption kinetics on solids is connected with the famous and commonly used empirical expression known in the literature as the Elovich equation [35]. This equation is more effective for explaining the kinetic behavior of chemical sorption systems [45]. In 1934, Zeldovich and Zeldovich [46] and Roginskii [47]

Table 2
Used adsorption kinetic equation

	Equation	Integrated from	Constants
Lagergren first-order [42]	$\frac{dq_t}{dt} = k_1(q_e - q_t)$	$\log(q_e - q_t) = \log q_e - \frac{k_1}{2.303} t$	$k_1 (\text{min}^{-1})$
Pseudo-second-order [43]	$\frac{dq_t}{dt} = k_2(q_e - q_t)^2$	$\frac{t}{q_t} = \frac{1}{k_2 q_e^2} + \frac{1}{q_e} t$	$k_2 (\text{g mg}^{-1} \text{min}^{-1})$
Elovich [46–48]	$\frac{dq_t}{dt} = \alpha e^{-\beta q_t}$	$q_t = \frac{1}{\beta} \ln(\alpha \beta) + \frac{1}{\beta} \ln t$	$\alpha (\text{mg g}^{-1} \text{min}^{-1}) \beta (\text{mg g}^{-1})$
Intraparticle diffusion [49]	$q_t = k_{int} t^{1/2}$		$k_{int} (\text{mg g}^{-1} \text{min}^{-1/2})$

found that the rate of adsorption of CO on finely divided MnO₂ between –78 and –39°C decreases exponentially with the increase of the amount (or fraction) q of gas adsorbed. The same equation was found by Elovich and Zhabrova [48] to apply up to 90–95% of the slow adsorptions of H₂ and of C₂H₄ with Ni-catalyzed at low temperatures. These authors also indicated the procedure for their equation and for determining the parameters α and β from the experimental data. Here, α is the degree of the initial adsorption and β is a constant related to surface coverage and activation energy of chemisorption.

In the industrial usage of adsorbents, the time dependence of adsorption on solid surfaces is known as adsorption kinetics. With the development of the theory of equilibria of adsorption on heterogeneous solid surfaces, the theory of adsorption–desorption kinetics on heterogeneous surfaces was also developed. Adsorption kinetics is determined by the following stages:

- (1) Diffusion of molecules from the bulk phase toward the interface space (so-called external diffusion);
- (2) Diffusion of molecules inside the pores (internal diffusion);
- (3) Diffusion of molecules in the surface phase (surface diffusion); and
- (4) Adsorption–desorption elementary processes.

In the case of sorption kinetics on microporous solids, a series of other mechanisms may additionally take place, *sui generis*. Diffusion in micropores carries the character of activated diffusion as described by Weber and Morris [49]. Before sorbing species can enter micropores, the penetration of surface barriers may be necessary. When adsorption systems fit the Langmuir isotherm equation that means the adsorbent has a nonporous and macroporous character. For nonporous and macroporous solids the internal diffusion may be neglected. In this case, the adsorption kinetics is determined by external diffusion and molecular adsorption–desorption processes. The Langmuirian kinetics, based on the ideal monolayer adsorbed model, proved to be deceptive for most real adsorption systems that include structurally high porous and energetically heterogeneous solids. On the other hand, the adsorption–desorption kinetics theories are technologically extremely important, because the diffusion of adsorbed particles on solid surfaces is a phenomenon of great importance in catalysis, metallurgy, microelectronics, material science, and numerous other scientific and technological applications [35].

2.6. Error analysis

Linear regression is one of the most viable tools for defining the best-fitting relationship quantifying the distribution of adsorbates, mathematically analyzing adsorption systems and verifying the consistency, and theoretical assumptions of an isotherm model [32]. Concomitant with the development of computer technology, the progression of nonlinear isotherm modeling has been extensively facilitated. Contrary to the linearization models, nonlinear regression usually involves the minimization or maximization of error distribution between the experimental data and the predicted isotherm based on its convergence criteria [39]. In this study, two error functions, the coefficient of determination and nonlinear chi-square test were used for analyzing the adsorption system.

Coefficient of determination, which represents the percentage of variability in the dependent variable (the variance about the mean), is employed to analyze the fitting degree of isotherm and kinetic models with the experimental data [32]. Coefficient of determination is defined as [44]

$$r^2 = \frac{\sum (q_{e,\text{meas}} - \overline{q_{e,\text{calc}}})^2}{\sum (q_{e,\text{meas}} - \overline{q_{e,\text{calc}}})^2 + (q_{e,\text{meas}} - q_{e,\text{calc}})^2} \quad (4)$$

where $q_{e,\text{meas}}$ (mg/g) is the amount of dye exchanged by the surface of red pine sawdust obtained from experiment, $q_{e,\text{calc}}$ the amount of dye obtained by isotherm models, and $\overline{q_{e,\text{calc}}}$ the average of $q_{e,\text{calc}}$ (mg/g). Its value may vary from 0 to 1, and the higher the r^2 values, the more useful the model. Essentially, r^2 tells us how much better we can predict $q_{e,\text{meas}}$ using the model and computing $q_{e,\text{calc}}$ than by just using the mean $q_{e,\text{calc}}$ as a predictor.

Nonlinear chi-square test is a statistical tool necessary for the best fit of an adsorption system, obtained by judging the sum squares differences between the experimental and the calculated data, with each squared difference being divided by its corresponding value (calculated from the models). Small χ^2 value indicates its similarities while a larger number represents the variation of the experimental data [32,40].

$$\chi^2 = \sum_{i=1}^n \frac{(q_{e,\text{calc}} - q_{e,\text{meas}})^2}{q_{e,\text{meas}}} \quad (5)$$

3. Adsorption thermodynamic

Thermodynamic parameters such as Gibb's free energy (ΔG°), enthalpy change (ΔH°), and change in

entropy (ΔS°) for the adsorption of dye on red pine sawdust were determined using the following equations

$$\Delta G^\circ = \Delta H^\circ - T\Delta S^\circ \quad (6)$$

$$\Delta G^\circ = -RT \ln(K_L) \quad (7)$$

$$K_L = \frac{q_e}{C_e} \quad (8)$$

$$\log\left(\frac{q_e}{C_e}\right) = \frac{\Delta S^\circ}{2.303 R} - \frac{\Delta H^\circ}{2.303 RT} \quad (9)$$

where q_e is the amount of dye adsorbed per unit mass of pine cone (mg/g), C_e is equilibrium concentration (mg/L), T is temperature in K, and R is the gas constant (8.314 J/molK). Considering the relationship between ΔG° and K_L , ΔH° and ΔS° were determined from the slope and intercept of the van't Hoff plots of $\log(K_L)$ vs. $1/T$. Negative values of ΔG° confirm the feasibility of the process and the spontaneous nature of the adsorption [50–52]. In general, the ΔH° value of physisorption is lower than 40 kJ/mol [50]. The positive value of ΔH° indicates that the adsorption reaction was endothermic [50,53,54]. The negative entropy change (ΔS°) for the process was caused by the decrease in degree of freedom of the adsorbed species [55].

4. Results and discussion

4.1. Effect of particle size

Fig. 1 shows the experimental results obtained from a series of experiments performed using five different pine sawdust particle sizes in the range (≤ 53 , 53–75, 75–90, 90–150, and 150–500 μm). As shown in

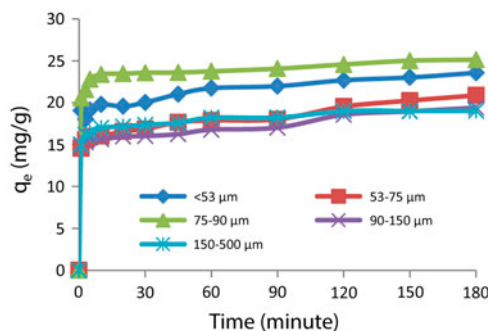


Fig. 1. The effects of adsorbent size on the AB256 sorption (pH: 6.3, $C_0 = 100 \text{ mg L}^{-1}$, temperature: 298 K, dose: 1 g/100 ml, contact time: 180 min., stirring rate: 600 rpm).

Fig. 1, in general, the adsorption capacity increases with decrease of the particle size. The observations are in line with the results obtained by Deniz and Karaman [12]. On the other hand, small sawdust particles could be aggregated to form larger particles. As for a heterogeneous system, many more factors are involved because it is a comprehensive impact of adsorption on the red pine sawdust, and it is hard to tell which factor might be predominant and how to balance them. Decrease in the particle size would lead to an increase in surface area and the increase in the adsorption opportunity at the outer surface of the pine sawdust. In addition, adsorbed dye molecules onto external surfaces of the red pine sawdust may be subjected to diffusion from external surface into pores of the sawdust adsorbent. The diffusional resistance to mass transfer is greater for large particles. Because of various factors, such as diffusional path length or mass transfer resistance, contact time, and blockage, sections of the particle may not be utilized for adsorption. Consequently, the adsorption capacity of large particles may be low [3]. On the other hand, when large particle's adsorption capacity is higher, it can be said that adsorbent size is not small enough to slip into the intraparticle or steric hindrance dominant factor at adsorption process. In this case, it can be said that adsorption occurs more favorably on the outer surface. In relatively small particles such as metal ions, intraparticle diffusion may be the dominant factor for adsorption. Optimum particle size ranges can be observed in 75–90 μm range. In these size ranges, capacities were determined as 25 mg dye/g red pine sawdust for AB256 dye.

4.2. Effect of pH

The pH of the aqueous solution is one of the important controlling parameters in the sorption process of textile dyes. The pH at the zero point of charge (pH_{zpc}) of Turkish red pine tree sawdust was found to be 6.3. At this pH, red pine sawdust particles are naturally charged, and the surface charge of the adsorbent is positive when the media pH is below the pH_{zpc} value while it is negative at a pH over the pH_{zpc} [3]. The effect of pH was studied in the pH ranges of 2–11 and results are shown in Fig. 2. The adsorption capacity increases significantly with a decrease in the pH. The maximum dye removals were observed at pH 2. At this pH value, the red pine sawdust surface charged positively, hence solution pH is below the pH_{zpc} . Because the molecular structure of dyes is unknown, it is hard to tell which part of the dyes interacted with adsorbent surface. It is very likely that positively charged red pine sawdust particle

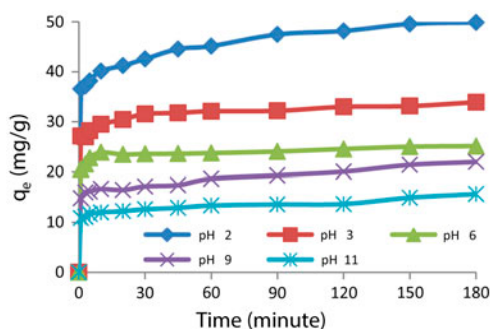


Fig. 2. The effects of pH on AB256 adsorption ($C_0=100 \text{ mg L}^{-1}$, 298 K, dose: 1 g/100 ml, stirring rate: 600 rpm, particle size: 75–90 μm).

surfaces would lead to increased adsorption of dye anions. Another possibility is that with a decreasing pH, dyes charges are mainly neutral; hence, it could be adsorbed by hydrogen bonding mechanism along with ion exchange. The maximum removal for AB256 with red pine sawdust was observed at pH 2. The amounts of adsorbed dye for AB256 increased from 49.9 to 15.6 mg/g with a decrease in pH from 11 to 2.

4.3. Effect of stirring rate

In order to understand the effect of stirring rates on the adsorption of working dyes onto red pine sawdust, experiments were carried out in batch systems with different stirring rates changing from 200 to 600 rpm. Obtained results are shown in Fig. 3.

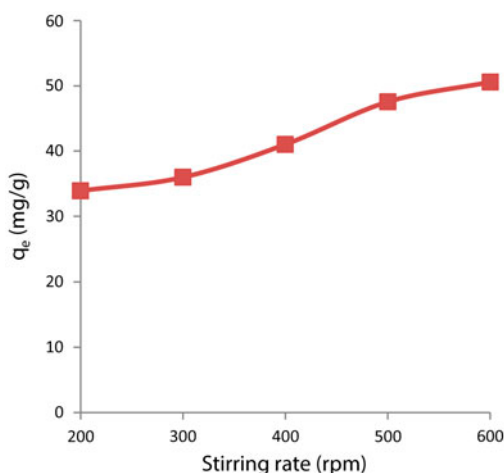


Fig. 3. The effects of stirring rate on AB256 adsorption ($C_0=100 \text{ mg L}^{-1}$, 298 K, dose: 1 g/100 ml, contact time: 180 min., pH 2, particle size: 75–90 μm).

It can be seen that the increase in stirring rate leads to a large increase in AB256 adsorption capacities, from 33.9 to 50.6 mg g^{-1} . This situation can be explained by the fact that with increasing stirring rates mobility of the system normally increased. At the same time, it is expected that the intraparticle diffusion speed increased, hence the number of free active sites of the red pine sawdust particle were higher than at low rpms. For further experiments 600 rpm stirring rate was selected.

4.4. Effect of adsorbent dose

The effect of the adsorbent dosage on adsorptions of AB256 on red pine sawdust is shown in Fig. 4. Red pine sawdust dosage was varied between 0.5 and 3 g/L with 0.5 g/L steps and equilibrated for 180 min. It can be seen from Fig. 4 that the removals of dyes increased with an increase in adsorbent dosage. The efficiency was 51% at the adsorbent concentration of 10 g/L, while it varied from 51 to 61% at adsorbent concentrations of 10–30 g/L for AB256, respectively. Although there was a triple increase in adsorbent dosage, the

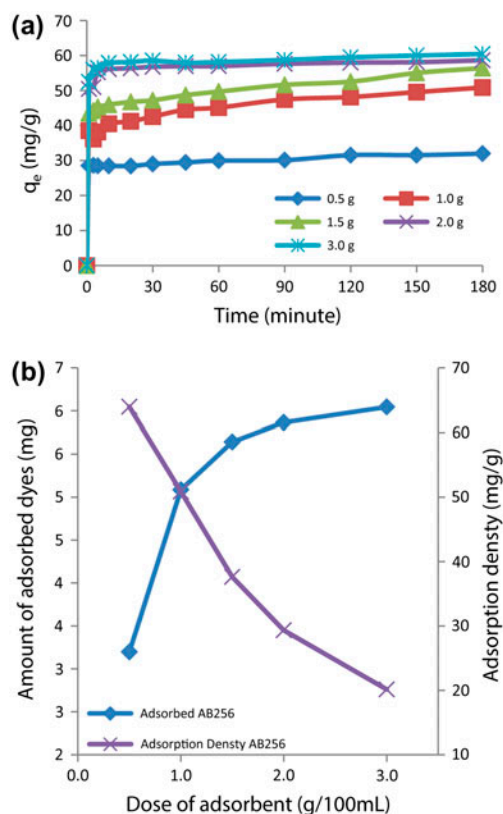


Fig. 4. The effects of sorbent dosage on the AB256 adsorption (a) and adsorption density (b) ($C_0 = 100 \text{ mg L}^{-1}$, 298 K, pH 2, particle size: 75–90 μm , 600 rpm, 100 mL).

removal greater than 10 g/L increased only up to about 10%. By increasing the red pine sawdust dose the amount of adsorbed dye increases but adsorption and adsorption densities decrease. This is because, the number of available adsorption sites increases by increasing the adsorbent dose. In addition, aggregation of particles may have a reductive impact on adsorption density. This situation will reduce the surface area of adsorbents and increase the diffusion path length. Thus, the equilibrium concentration is considered to be 10 g/L for red pine sawdust.

4.5. Effect of contact time and initial dye concentration

The preliminary experiments showed that the adsorption of AB256 is fast at the initial stages and becomes slower near the equilibrium. Fig. 5 presents the plots of AB256 removal vs. contact time for red pine sawdust at initial concentrations between 25 and 300 mg/L at 298 K with a contact time of 180 min. The rates of dye removal for both dyes are very rapid until three minutes and the plot flattens thereafter, as can be seen from Fig. 5. It can be seen that there was no considerable change for adsorption of AB256 after 120 min for varied initial concentrations. The equilibrium times are independent of each initial dye concentration. With the increase in the initial dye concentration, the efficiency increases. This phenomenon can be explained by the high adsorption capacity of red pine sawdust. When comparing to our previous report [3] made with another metal complex dye, AY132, it can be observed that AB256 adsorption capacity was higher than AY132 adsorption capacity. This can be explained by the fact that the molar weight of AB256 is higher than AY132. Another reason could be that the molecular structure of AB256 is more branched than AY132, causing diffusion

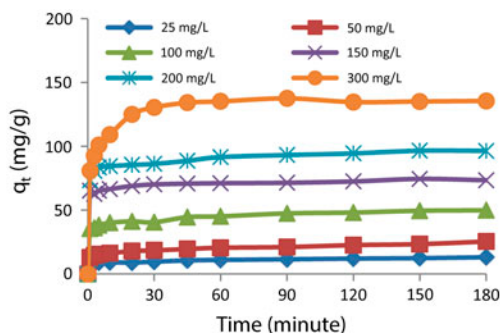


Fig. 5. The effects of contact time and initial dye concentration on AB256 adsorption ($C_0 = 25\text{--}300\text{ mg L}^{-1}$, 298 K, contact time: 180 min., pH2, particle size: 75–90 μm , 600 rpm, 100 mL, dose: 1 g).

difficulty of dye into pores. Because the molecular formula of used dyes is unknown, it is difficult to provide an exact reason for this phenomenon.

4.6. Kinetics of the adsorption

To design a suitable adsorption system, adsorption kinetics is the key factor, and choosing appropriate kinetic equations when modeling the system correctly is equally important. Here, kinetic isotherm constants of worked models were determined by nonlinear regression. Kinetic parameters for four kinetic models, chi-square values (χ^2) and correlation coefficients (r^2) were calculated and are listed in Table 3. The values of χ^2 of pseudo-second-order kinetic model for AB256 dye are very high, followed by those of the pseudo-first-order equation, Elovich equation, and intraparticle diffusion equation, respectively. In the pseudo-second-order equation, the correlation coefficients were higher than 0.9995 and chi-square values were lower than 0.0977. Here, due to high r^2 and low χ^2 values, the pseudo-second-order is the predominant kinetic model for AB256 dye sorption by red pine sawdust. Moreover, the equilibrium sorption capacities for pseudo-second-order are slightly more reasonable than those of the pseudo-first-order when comparing predicted results with experimental data, because all of the equilibrium sorption capacities, q_1 , of pseudo-first-order are lower than experimental results. As can be seen in Table 3, q_e values increased from 13.12 to 135.6 mg/g with an increase in the initial dye concentration from 25 to 300 mg/L with red pine sawdust (1 g/l for AB256 dye). The pseudo-second-order equation's calculated the equilibrium sorption capacities, q_2 , fit the experimental data. The maximum deviation was observed as about 6% at 300 mg/L initial concentration. These suggest that the pseudo-second-order sorption mechanism is predominant and that the overall rate of the acid dyes sorption process appear to be controlled by the chemical process. Similar results have also been observed in biosorption of dyes BB69, AB25, methylene blue, bismarck brown, and acridine orange on wood [56,57]. For the pseudo-second-order model, the rate constant, k_2 , decreases with an increasing of initial dye concentration, while the calculated sorption capacity, q_2 , increases with an increasing of initial dye concentration.

The plotting of AB256 dye sorption using red pine sawdust in Fig. 6, shows that kinetics of acid dye sorption consisted of two phases; an initial rapid phase where sorption was fast and a second slower phase where equilibrium uptake was achieved. A rapid adsorption onto external surface of the red pine sawdust is the first phase. The second phase is the

Table 3
Kinetic parameters for the effects of sorbent particle size, pH, dose, and initial concentration on the sorption of AB256 onto red pine sawdust

Parameters	First-order kinetic equation				Second-order kinetic equation				The Elovich equation				Intraparticle diffusion equation			
	$q_{e,exp}$ (mg/g)	q_1 (mg/g)	k_1 (1/min)	r^2	x^2	q_2 (mg/g)	k_2 (g/(mg min))	r^2	x^2	α (mg g ⁻¹ min ⁻¹)	β (mg g ⁻¹)	r^2	x^2	k_{int} (mg g ⁻¹ min ^{-1/2})	r^2	x^2
≤53 μm	19.02	17.86	1.842	0.9790	0.3594	18.19	0.2344	0.9916	0.1411	119.1 × 10 ⁹	1.289	0.9340	2.3191	2.431	0.2257	73.08
53–75 μm	19.40	18.54	2.215	0.9872	0.2229	18.78	0.3381	0.9941	0.1017	206.1 × 10 ¹²	2.007	0.9992	0.0141	2.099	0.2865	55.58
75–90 μm	20.87	19.34	1.703	0.9718	0.5419	19.78	0.1792	0.9900	0.1897	185.8 × 10 ¹⁷	2.095	0.9716	0.6796	2.568	0.2234	75.61
90–150 μm	23.56	22.93	1.311	0.9880	0.2750	23.47	0.1124	0.9992	0.0182	321.1 × 10 ⁵	1.151	0.9465	0.8292	2.136	0.4220	48.30
150–500 μm	25.13	23.73	1.977	0.9814	0.4261	24.13	0.2012	0.9924	0.1713	710.1 × 10 ⁴	0.980	0.9564	0.7377	2.309	0.4330	51.74
pH 2	49.87	46.416	0.0915	0.9832	1.950	52.33	0.0020	0.9999	0.0159	10.23	0.2025	0.9847	10.60	4.986	0.8343	29.91
pH 3	33.90	31.844	0.1033	0.9843	1.189	35.62	0.0034	0.9999	0.0065	11.57	0.1563	0.9802	1.336	3.445	0.8094	24.12
pH 6	25.13	23.478	0.1046	0.9832	0.912	26.27	0.0047	0.9999	0.0267	8.491	0.2109	0.9813	0.888	2.544	0.8100	17.92
pH 9	21.97	21.527	0.0273	0.9971	0.214	27.49	0.0009	0.9996	0.0157	3.319	0.2734	0.9580	9.241	1.807	0.9661	4.82
pH 11	15.64	15.245	0.0290	0.9964	0.319	19.63	0.0013	0.9919	0.6261	2.165	0.3746	0.9618	9.384	1.278	0.9357	5.75
0.5 g	31.98	29.773	0.1287	0.9828	1.130	32.98	0.0047	0.9999	0.0052	29.00	0.1302	0.9749	28.84	3.271	0.7774	27.93
1.0 g	50.87	46.591	0.0904	0.9820	1.998	52.64	0.0020	0.9997	0.0231	15.21	0.1057	0.9868	1.613	5.005	0.8400	29.13
1.5 g	56.43	52.060	0.0810	0.9837	2.270	59.14	0.0016	0.9998	0.0583	15.94	0.0949	0.9873	2.333	5.533	0.8545	28.46
2.0 g	58.66	53.728	0.0780	0.9840	2.140	61.30	0.0014	0.9998	0.0207	15.70	0.0912	0.9885	2.250	5.683	0.8593	28.09
3.0 g	60.45	55.530	0.0653	0.9866	1.940	64.17	0.0011	0.9997	0.0385	14.38	0.0885	0.9885	3.571	5.740	0.8798	23.27
25 mg/L	13.12	12.34	0.3455	0.9779	0.473	13.02	0.0389	0.9995	0.0074	13.12	0.1579	0.8633	78.22	1.394	0.5952	23.28
50 mg/L	25.45	23.88	0.1837	0.9813	0.926	25.84	0.0092	0.9999	0.0023	17.79	0.2351	0.9620	1.773	2.662	0.7156	30.51
100 mg/L	49.87	46.41	0.0917	0.9831	1.900	52.41	0.0020	0.9999	0.0077	15.31	0.1062	0.9854	1.672	4.984	0.8335	30.07
200 mg/L	96.47	89.76	0.0786	0.9862	3.128	102.9	0.0009	0.9999	0.0367	26.30	0.0546	0.9864	4.121	9.480	0.8520	48.70
300 mg/L	135.6	127.3	0.0790	0.9864	4.266	144.7	0.0006	0.9999	0.0977	37.00	0.0383	0.9863	5.337	13.43	0.8482	71.08

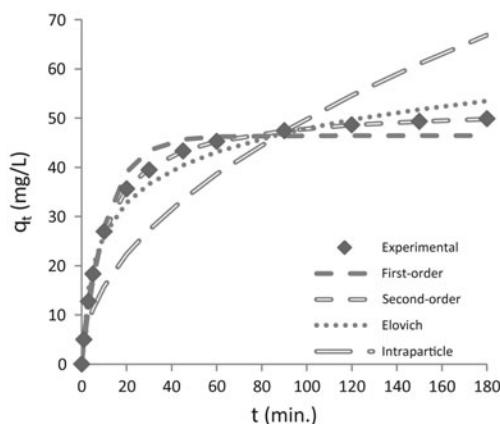


Fig. 6. The measured and nonlinear modeled time profiles for biosorption of the AB256 dye at 100 mg/L initial dye concentration onto red pine sawdust at a temperature of 298 K.

gradual sorption stage from outer surface to pores before the dye uptake reaches equilibrium. The pseudo-first-order considers the rate of occupation of adsorption sites to be proportional to the number of unoccupied sites. Furthermore, a widely used equation to describe the kinetics of chemisorption of gas on solids was proposed by Elovich [48]. The Elovich model is slightly applicable for describing AB256 adsorption onto red pine sawdust. This suggests that AB256 adsorption system's character may be chemisorption involving valence forces through sharing or exchange of electrons between red pine sawdust particles and AB256 dye molecules [35]. Because the cell walls of red pine sawdust are mainly formed of cellulose and lignin and many hydroxyl containing compounds like tannins or other phenolic compounds, the AB256 sorption is usually controlled either by intraparticle or surface diffusion [58].

4.7. Adsorption isotherms

The five most common isotherms were selected for this study, namely the Langmuir, Freundlich, Tempkin, Dubinin–Radushkevich, and Redlich–Peterson isotherms. A comparison of two linear and nonlinear solutions to the Langmuir isotherm was carried out first. Then, Freundlich, Tempkin, Dubinin–Radushkevich, and Redlich–Peterson were applied to the experiment of two dyes sorption on red pine sawdust. Here, at linear forms Pearson's correlation coefficient (r^2) error function and at nonlinear solutions Pearson's chi-square (χ^2) error function were taken into consideration and then for others, the error function was calculated. In addition, in the nonlinear Langmuir solution, where

the predicted values generated from a model are different from linear regression, an r^2 value can be calculated between the measured q_e and modeled q_e data values. In this case, the value is not directly a measure of how good the modeled values are, but rather a measure of how good a predictor might be when constructed from the modeled values. This usage is specifically the definition of the term "coefficient of determination": the square of the correlation between two variables.

Linear regression is one of the most acceptable tools defining the best-fitting relationship quantifying the distribution of adsorbates, mathematically analyzing the adsorption systems and verifying the consistency, and theoretical assumptions of an isotherm model. Contrary to the linearization models, nonlinear regression usually involves the minimization or maximization of error distribution (between the experimental data and the predicted isotherm) based on its convergence criteria. However, there is also an opinion about nonlinear regression not being statistically correct. This opinion is based on experimental errors in both the dependent and independent variables in the isotherm equations [30]. In this case, r^2 values for both linear forms of Langmuir isotherm were significantly different as summarized in Table 1. When using only the linear forms of Langmuir isotherms for comparison, Lineweaver–Burk linear form was suitable with the Langmuir linear form for the experimental data. Contrary to this, when considering χ^2 values, the linear form of Langmuir was most suitable between the two linearized forms. Even though the most suitable isotherm for the data-set was the Lineweaver–Burk form, the differences between the two linear forms of Langmuir isotherms were significantly in agreement with experimental results. Each linear equation has different axial settings individually, so that would alter the result of a linear regression and influence the determination process. For this reason, it is not appropriate to use r^2 of linear regression analysis for comparing the best fitting of Freundlich, Tempkin, Dubinin–Radushkevich, and both linear Langmuir isotherms. χ^2 (Pearson's chi-square) error function analysis could be a better method.

The chi-square distribution value of the Dubinin–Radushkevich isotherm was significantly higher than each value for AB256 dye adsorption onto red pine sawdust. Based on the χ^2 values, as indicated in Table 4, it can be said that the nonlinear method is the most reliable method for solution of the Langmuir isotherm. Beyond that, the best fitting isotherm of the five studied isotherms is the Redlich–Peterson isotherm for AB256 adsorption. χ^2 statistical tests were not able to reveal the more appropriate between

Table 4
Isotherm constants for dyes adsorption onto red pine sawdust

Isotherm	K_L (L/g)	a_L (L/mg)	Q_{\max} (mg/g)	R_L	r^2	x^2
Lineweaver–Burk linear	0.1130	0.0025	45.17	0.9411–0.5712	0.9995	0.0272
Langmuir linear	0.1110	0.0021	53.94	0.9511–0.6183	0.9784	0.0057
Nonlinear regression	0.1109	0.0020	54.16	0.9513–0.6194	0.9996*	0.0057
Freundlich	K_f (L/g)	n			r^2	x^2
	6.985	1.109			0.9988	0.0506
Tempkin	A (L/g)	B (j/mol)			r^2	x^2
	0.0822	4.539			0.9190	2.474
Dubinin–Radushkevich	β (mmol/j) ²	q_m (mmol/g)	E (kJ/mol)		r^2	x^2
	0.5166	7.783	0.9838		0.7572	23.65
Redlich–Peterson	K (L/g)	a (L/mg)	β		r^*	x^2
	0.1110	0.0021	0.9999		0.9913	0.0057

*These values are calculated by simulating.

Redlich–Peterson and Langmuir model nonlinear approaches (see Table 4). Coefficient of determination (r^2) was able to point to the Langmuir nonlinear method as the most appropriate (having r^2 0.9996 value). Because of the Redlich–Peterson isotherm's β value is equal to 0.9999 for each dye, the most reliable Langmuir isotherm solution is nonlinear regression. These confirm the monolayer coverage of dyes onto red pine sawdust particles and also the homogeneous distribution of active sites on the adsorbent, since the Langmuir equation assumes that the surface is homogeneous. According to the Langmuir nonlinear method, monolayer saturation capacity of AB256 dyes onto red pine sawdust was determined as 54.16 mg/g.

The calculated R_L values at different initial dye concentrations are shown in Fig. 7. Dimensionless constant, R_L indicates the shape of the isotherms to be either unfavorable ($R_L > 1$), linear ($R_L = 1$), favorable ($0 < R_L < 1$), or irreversible ($R_L = 0$). It was observed that R_L values were determined between 0.9513 and

0.6194 for AB256 dyes. This indicated that adsorptions were more favorable for the higher initial dye concentrations than for the lower ones. Langmuir isotherm constants, r^2 , and x^2 values are listed in Table 4. Freundlich isotherm is widely applied in heterogeneous systems especially for organic compounds or highly interactive species on activated carbon and molecular sieves. The slope ($1/n$) ranges between 0 and 1 which is a measure of adsorption intensity or surface heterogeneity, and it becomes more homogeneous when its value gets closer to one. Slope of AB256 dye was determined as 0.9017. These results are further evidence of the surface homogeneity. Tempkin isotherm showing less agreement with the experimental data, x^2 values 2.474 for AB256; hence, it can be considered as an indication of the surface not being heterogeneous. Here, initial concentrations having relatively high values (Table 4 Langmuir's R_L values), caused relatively low x^2 values for adsorption systems.

Dubinin–Radushkevich isotherm constant, β (mmol²/J²), has been used to calculate the mean free energy (E) of sorption per mole of the adsorbate. E value was calculated as 0.9838 for AB256. Because of E in the range of $8 < E < 16$ KJ/mol, adsorption is governed by ion exchange mechanism [3,38]. Using Langmuir's Q_{\max} (mg/g) and Dubinin–Radushkevich's q_m (mmol/g) values, unknown molecular weight of dyes can be calculated approximately. The reason is, especially with the Dubinin–Radushkevich isotherm, the compliance of isotherms with experimental data is low. Molecular weights of dyes were calculated as ~6958.8 g/mol for AB256. The Redlich–Peterson isotherm parameters K (L/g), a (L/mg^{1-1/A}), and β can be seen in Table 1. Because of isotherm unitless constant β values having 0.9999 and = 1 for each dye, adsorption isotherm fits Langmuir isotherm. A comparison is also made between the experimental data and worked

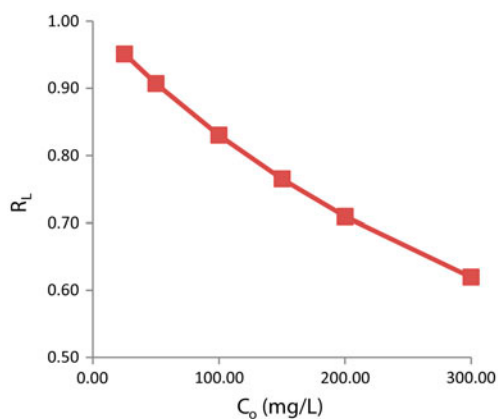


Fig. 7. Plots of separation factor vs. initial dye concentrations.

isotherms plotted in Fig. 8. As can be seen from Table 4, the Langmuir, Freundlich, and Redlich–Peterson isotherms equations show sufficient compliance with the experimental results. Despite the fact that the Dubinin–Radushkevich isotherm represents adsorption systems at low concentrations, the Tempkin isotherm was generally in more agreement with experimental data than the Dubinin–Radushkevich isotherm. Based on Fig. 8, it can be said that the Redlich–Peterson isotherm generates a satisfactory fit with the experimental data in all data points.

4.8. Effect of temperature on adsorption

In order to understand the effect of temperature on adsorption of AB256 dye onto red pine sawdust, experiments were conducted at temperatures of 298, 313, 333, and 353 K, and the results are shown in Fig. 9. As shown in Fig. 9, the results indicate that each amount of adsorbed dye decreases with an increase in temperature. For example, for an initial AB256 dye concentration of 100 mg/L, when increasing initial solution temperature from 298 to 353 K, the amount of dye adsorbed per unit weight of dye decreases from 55.89 to 51.04 mg/g. The decrease in the adsorption capacity at increased temperatures indicates the exothermic nature of the adsorption process of AB256 dyes onto red pine sawdust.

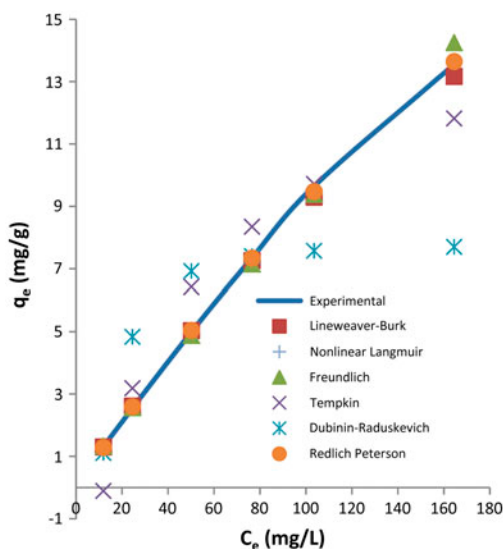


Fig. 8. Equilibrium curves for adsorption of AB256 onto red pine sawdust ($C_0 = 25\text{--}300\text{ mg L}^{-1}$, 298 K, 180 min., pH2, 75–90 μm particle size, 600 rpm, 100 mL, 1 g adsorbent).

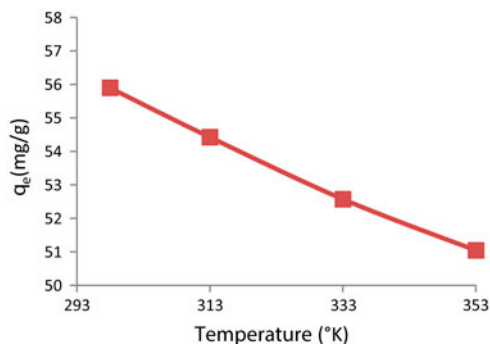


Fig. 9. Effect of temperature on adsorption of AB256 dye ($C_0 = 100\text{ mg L}^{-1}$, 180 min., pH2, 75–90 μm particle size, 600 rpm, 100 mL, 1 g adsorbent).

4.9. Determination of thermodynamic parameters

The plot of $\ln K_d$ against $1/T$ (in Kelvin) should be linear from which ΔH° and ΔS° were calculated from the slope and intercept, respectively. The slope of the van't Hoff plot is equal to $-\Delta H^\circ/R$ and its interception is equal to $\Delta S^\circ/R$ from Eq. (10). The van't Hoff plot for the adsorption of dyes onto red pine sawdust is given in Fig. 10. Thermodynamic parameters obtained are given in Table 5. As shown in the table, the negative values of ΔG° at different temperatures indicate the spontaneous nature of the adsorption process.

The negative value of ΔH° suggests the exothermic nature of each adsorption system. Generally, when ΔH° value is smaller than 40 kJ/(mol K), this interaction is assumed as weak interaction or physisorption [59]. Based on this study, ΔH° values were determined as $-3.116\text{ kJ}/(\text{mol K})$ for AB256, and this suggests that the adsorption of dyes onto red pine sawdust was a physisorption process. The negative value of ΔS°

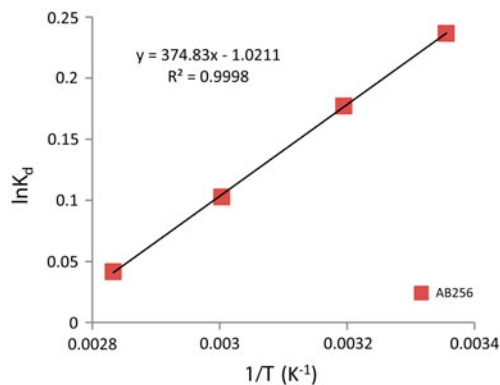


Fig. 10. Van't Hoff plot of $\ln K_d$ vs. $1/T$ for the estimation of thermodynamic parameters.

Table 5
Thermodynamic parameters for the adsorption of AB256 dye onto red pine sawdust

ΔH° (kJ/mol K)	ΔS° (J/mol K)	ΔG° (kJ/mol K)			
		298 K	313 K	333 K	353 K
-3.116	-8.49	-586.44	-461.29	-284.86	-122.11

suggests the decreased randomness at the solid/solution interface during the adsorption of AB256 dye red pine sawdust. As is well known, all systems move toward minimum energy and maximum randomness. Here, for each dye system, although randomness has decreased, the tendencies of systems toward minimum energy seem to be the dominant.

4.10. Process design

Best fitting adsorption isotherm equation can be used for designing single-stage batch adsorber systems [60,61]. A representation of the system can be seen in Fig. 11. It was designed for different solution volumes. The design objective was to reduce the dye solution of volume V , L from an initial dye concentration of $C_0 - C_1$ (mg/L). The amount of adsorbent is M and the solute loading on the adsorbent changes from q_0 (mg/g) to q_1 (mg/g). At time $t = 0$, $q_0 = 0$, and as time proceeds to the mass balance, the dye removed from the liquid equates to that picked up by the solid. The mass balance equation for the sorption system in Fig. 11 can be written as equation

$$V(C_0 - C_1) = M(q_1 - q_0) = Mq_1 \tag{10}$$

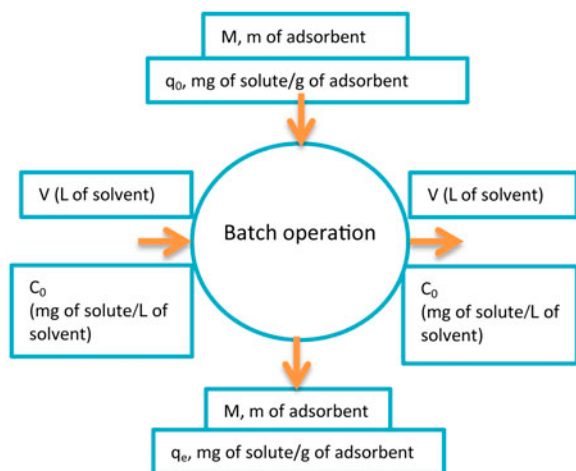


Fig. 11. Schematic representation of the single-stage batch adsorber system.

When the system reaches equilibrium, C_1 and q_1 will change to C_e and q_e , respectively. Since, the equilibrium studies confirm that the equilibrium data for AB256 onto red pine sawdust follow a Langmuir isotherm equation substituted with q_e in Eq. (1), it can be rearranged as

$$\frac{M}{V} = \frac{C_0 - C_1}{q_e} = \frac{C_0 - C_e}{\left[\frac{K_L C_e}{1 + K_L C_e} \right]} \tag{11}$$

Fig. 12 shows a series of plots derived from Eq. (2) for adsorbent consumption for the different AB256 dye solution volumes. When the initial dye concentration of 100 g/m^3 is assumed, the required amount of red pine sawdust reduced the color content by 75%–99% at various volumes of effluents. For a single-stage adsorption system, the sawdust demonstrated the elimination capacity of the AB256 dye containing effluents. For example, 5 m^3 of solution is to be treated. The required masses of bentonite are 142.1, 187.7,

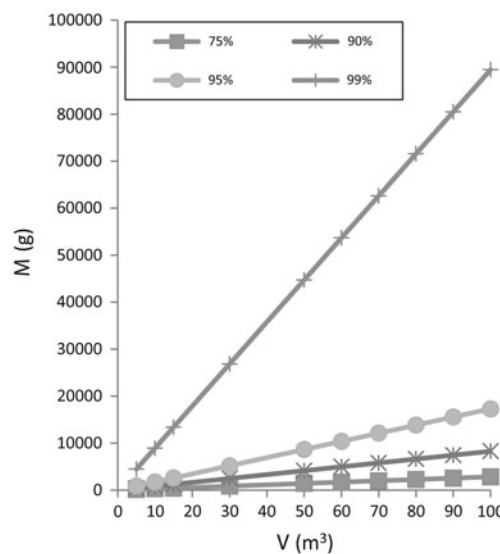


Fig. 12. Adsorbent mass (M) against volume of effluent (V) treated for various percentages of color removal at 100 g/m^3 initial AB256 concentration.

263.3, 414.0, 865.1, and 4471.2 kg for 75, 80, 85, 90, 95, and 99% dye removal, respectively.

Fig. 13 shows the required amount of sawdust to reduce the color content by 99% at various volumes of effluents that have different AB256 concentrations. For example, 50 m³ of solution is to be treated. The required amounts of sawdust to reduce the color content by 99%, increased from 26.57 to 492.3 kg with an increase in the initial AB256 concentration from 25 to 500 g/m³. The amount of sawdust required to remove 99% of dye from an aqueous solution can be predicted for any initial dye concentration for a fixed volume of

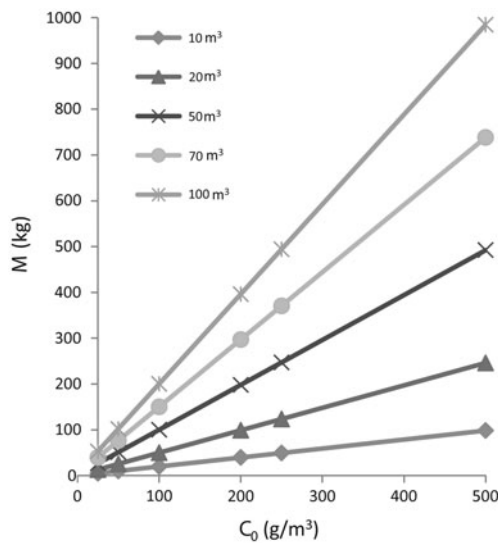


Fig. 13. Adsorbent mass (M) against initial MG concentration for 99% color removal at various volumes of effluent (V) treated.

effluent (V). Through such a projection, a real single-stage adsorption system can be designed.

4.11. Characterization

FTIR spectra of red pine sawdust and AB256 adsorbed red pine sawdust are illustrated in Fig. 14. The cell walls of pine sawdust mainly consist of cellulose, hemicelluloses, lignin, and many hydroxyl groups, such as tannins or other phenolic compounds [58]. Lignin is a polymer material built-up from the phenyl propane nucleus, an aromatic ring with a three-carbon side chain. Vanillin and syringaldehyde are the two other basic structural units of lignin molecules. Tannins are complex polyhydric phenols, which are soluble in water and have the property of precipitating protein (gelatin).

The comparison of the FTIR spectra shows that some peaks were shifted. In the case of the red pine sawdust, there is a strong peak at wavenumber 3,338 cm⁻¹ representing the single -OH stretching of phenol group of cellulose and lignin, and the peak at 2,886 cm⁻¹ indicates the presence of single -CH₂ stretching of aliphatic compound. The peaks like a saw sign around 2,000 cm⁻¹ indicate the presence of single -NH stretching. The appearance of peaks at 1,713 and 1,656 cm⁻¹ indicates the presence of C=O stretching of aldehyde group and C=C stretching of the phenol group, respectively. Whereas, the peaks at 1,590 and 1,507 cm⁻¹ in the spectrum of red pine sawdust can be due to C=C of benzene aromatic ring, peaks at 1,453 and 1,422 cm⁻¹ can be due to single -CH₂ bending and single -OH bending, respectively. The peaks at 1,397 and 1,315 cm⁻¹ show C-O-H bending and C-H in plane deformation. Peaks at 1,266 and 1,157 cm⁻¹ in the FTIR spectrum of sawdust can be

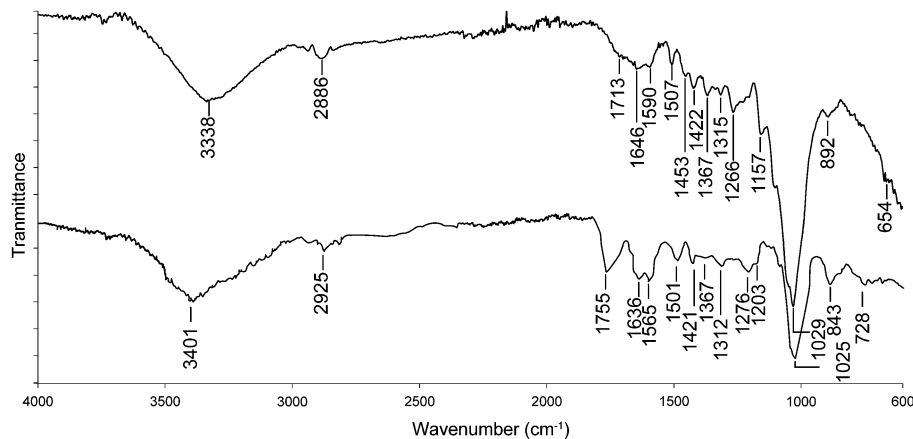


Fig. 14. FTIR spectra of sawdust and AB256 adsorbed sawdust.

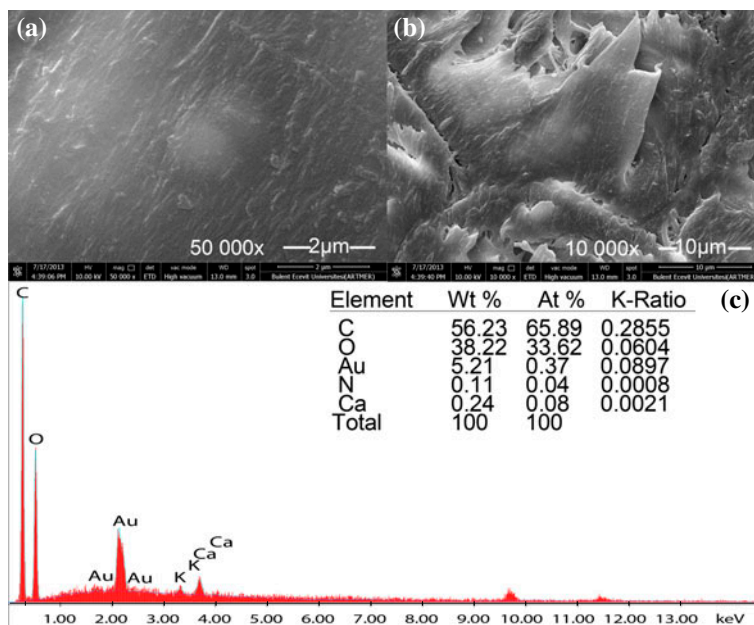


Fig. 15. FESEM micrograph of AB256 adsorbed, (a) natural, (b) red pine sawdust particles (10 kV), and EDX analysis (c).

due to C–O stretching of phenolic group and six-member cyclic ether group of cellulose, respectively. Typical wood cellulose gives characteristic of β -glycosidic linkages band at 892 cm^{-1} . Peak at 654 cm^{-1} represents C–C stretching. These wavenumber values are very close to those reported for pine sawdust by [16].

After adsorption of AB256, the peak at $1,775\text{ cm}^{-1}$ appeared, which indicated the presence of the carboxylic acid group since the AB256 solution was acidic. The interaction between AB256 and carboxylic, amino and hydroxyl groups was detected by the shift in wavenumber from $3,338$ to $3,401\text{ cm}^{-1}$. The peak in sawdust at $1,157\text{ cm}^{-1}$ that also represented C–N bending vibration had shifted to $1,203\text{ cm}^{-1}$ after AB256 adsorption. All the findings from FTIR spectra led to a conclusion that O and N-containing groups are the main adsorption sites for AB256. The characteristic of β -glycosidic linkages at 892 cm^{-1} in sawdust spectra shifted to 843 cm^{-1} due to AB256 adsorption. C–C stretching peak at 654 cm^{-1} disappeared and a new peak at 728 cm^{-1} was formed representing C–H out-of-plane bending absorption in aromatic ring.

The FESEM images at $50,000\times$ magnification of AB256 adsorbed red pine sawdust and at $10,000\times$ magnification of red pine sawdust are shown in Fig. 15(a) and (b). The micrograph of AB256 adsorbed red pine sawdust particles (Fig. 15(a)) reveals low porosity and irregular surface structure. Red pine sawdust has a macro porous structure due to the presence of large pores (Fig. 15(b)).

The elemental composition of red pine sawdust is shown in Fig. 15(c) inset Table (C: 56.23%, O: 38.22%, Nitrogen: 0.11%, Calcium: 0.25%). These are very similar to those measured for other wood materials [62–64]. The results of proximate analysis indicate that the ash content in sawdust (0.24%) reveals the presence of calcium oxide and, to a much lower extent, calcium carbonate.

5. Conclusions

In this study, the potential of red pine sawdust of *P. resinosa* as a natural biosorbent was investigated for removal of AB256 dye from aqueous solutions in the batch mode. The adsorbed amounts of dye increased with increasing particle size of red pine sawdust due to the steric hindrance of big dye molecules. There was no considerable change for removal of AB256 after 120 min of contact time for different initial concentrations. The equilibrium times are independent of each initial dye concentration. The biosorption kinetic of red pine sawdust for AB256 dyes was investigated and the pseudo-second-order kinetic model provided the best correlation with the experimental data. It can be said that the sorption capacity of AY132 [3] is higher than AB256 because of the ionic charges on the dyes and the character of the biomaterials. Nonlinear method of Langmuir isotherm equation was found to provide the closest fit with the equilibrium data for

AB256 dye, and the optimum parameter values were produced by nonlinear regression using the Pearson's chi-square error function.

The monolayer sorption capacity of the biosorbent for AB256 was found as 54.16 mg/g. The thermodynamic studies indicated that the sorption processes were favorable, exothermic, and minimum energy tendency driven. The randomness decreased at the solid/solution interface. Activation energies showed that AB256 adsorption onto the red pine sawdust was physical sorption. Assuming the batch adsorption to be a single-staged equilibrium operation, the separation process can be defined mathematically using the Langmuir isotherm constants to estimate the residual concentration of AB256 or amount of adsorbent for desired purification. It can be concluded that bentonite may be used as a low-cost, natural and abundant source for the removal of AB256, and might be an alternative to more costly materials.

Acknowledgment

The author is most grateful to Dr Emrah Bulut for his comments on the first version of this manuscript and for several valuable suggestions that have been included in the final form.

References

- [1] R. Helmer, I. Hespanhol, *Water Pollution Control: A Guide to the Use of Water Quality Management Principles*, E&FN Spon, London, 1997.
- [2] O.J. Hao, H. Kim, P.-C. Chiang, Decolorization of wastewater, *Crit. Rev. Env. Sci. Technol.* 30 (2009) 449–505.
- [3] M. Can, Biomaterials derived from renewable resources for the recovery of precious metals, *Res. J. Chem. Environ.* 17 (2013) 1–3.
- [4] V.K. Gupta, Suhas, Application of low-cost adsorbents for dye removal—A review, *J. Environ. Manage.* 90 (2009) 2313–2342.
- [5] N. Daneshvar, A.R. Khataee, M.H. Rasoulifard, M. Pourhassan, Biodegradation of dye solution containing Malachite Green: Optimization of effective parameters using Taguchi method, *J. Hazard. Mater.* 143 (2007) 214–219.
- [6] M.H. Vijaykumar, Y. Veeranagouda, K. Neelakanteshwar, T.B. Karegoudar, Decolorization of 1:2 metal complex dye Acid blue 193 by a newly isolated fungus, *Cladosporium cladosporioides*, *World J. Microbiol. Biotechnol.* 22 (2006) 157–162.
- [7] Z. Aksu, E. Balibek, Effect of salinity on metal-complex dye biosorption by *Rhizopus arrhizus*, *J. Environ. Manage.* 91 (2010) 1546–1555.
- [8] A. Demirci, M.B. Mutlu, A. Güven, E. Korcan, K. Güven, Decolorization of Textile Azo-metal Complex Dyes by a Halophilic Bacterium Isolated from Çamaltı Saltern in Turkey, *Clean: Soil Air Water* 39 (2011) 177–184.
- [9] F. Deniz, S. Karaman, Removal of an azo-metal complex textile dye from colored aqueous solutions using an agro-residue, *Microchem. J.* 99 (2011) 296–302.
- [10] L.-N. Du, B. Wang, G. Li, S. Wang, D.E. Crowley, Y.-H. Zhao, Biosorption of the metal-complex dye Acid Black 172 by live and heat-treated biomass of *Pseudomonas* sp. strain DY1: Kinetics and sorption mechanisms, *J. Hazard. Mater.* 205–206 (2012) 47–54.
- [11] K.K.H. Choy, G. McKay, Synergistic multilayer adsorption for low concentration dyes by biomass, *Chin. J. Chem. Eng.* 20 (2012) 560–566.
- [12] F. Deniz, S. Karaman, Removal of Basic Red 46 dye from aqueous solution by pine tree leaves, *Chem. Eng. J.* 170 (2011) 67–74.
- [13] T.K. Sen, S. Afroze, H.M. Ang, Equilibrium, kinetics and mechanism of removal of Methylene Blue from aqueous solution by adsorption onto pine cone biomass of *Pinus radiata*, *Water Air Soil Pollut.* 218 (2011) 499–515.
- [14] H. Zhang, Y. Tang, X. Liu, Z. Ke, X. Su, D. Cai, X. Wang, Y. Liu, Q. Huang, Z. Yu, Improved adsorptive capacity of pine wood decayed by fungus *Poria cocos* for removal of malachite green from aqueous solutions, *Desalination* 274 (2011) 97–104.
- [15] M.A.K.M. Hanafiah, W.S.W. Ngah, S.H. Zolkafly, L.C. Teong, Z.A.A. Majid, Acid Blue 25 adsorption on base treated *Shorea dasyphylla* sawdust: Kinetic, isotherm, thermodynamic and spectroscopic analysis, *J. Environ. Sci.* 24 (2012) 261–268.
- [16] D. Sidiras, F. Batzias, E. Schroeder, R. Ranjan, M. Tsapatsis, Dye adsorption on autohydrolyzed pine sawdust in batch and fixed-bed systems, *Chem. Eng. J.* 171 (2011) 883–896.
- [17] I. Langmuir, The adsorption of gases on plane surface of glass, mica and platinum, *J. Am. Chem. Soc.* 40 (1918) 1361–1403.
- [18] I. Langmuir, The constitution and fundamental properties of solids and liquids, *J. Am. Chem. Soc.* 38 (1916) 2221–2295.
- [19] O. Altun, H.Ö. Özbelge, T. Doğu, Use of general purpose adsorption isotherms for heavy metal-clay mineral interactions, *J. Colloid Interface Sci.* 198 (1998) 130–140.
- [20] H. Lineweaver, D. Burk, The determination of enzyme dissociation constants, *J. Am. Chem. Soc.* 56 (1934) 658–666.
- [21] G.S. Eadie, The inhibition of cholinesterase by physostigmine and prostigmine, *J. Biol. Chem.* 146 (2) (1942) 85–93.
- [22] G.S. Eadie, On the evaluation of the constants V_m and K_M in enzyme reactions, *Science* 116 (1952) 688.
- [23] B.H.J. Hofstee, On the evaluation of the constants V_m and K_M in enzyme reactions, *Nature* 184 (1959) 329–331.
- [24] G. Scatchard, The attractions of proteins for small molecules and ions, *Ann. N.Y. Acad. Sci.* 51 (1949) 660–672.
- [25] M.I. El-Khaiary, Least-squares regression of adsorption equilibrium data: Comparing the options, *J. Hazard. Mater.* 158 (2008) 73–87.
- [26] C.H. Bolster, G.M. Hornberger, On the use of linearized Langmuir equations, *Soil Sci. Soc. Am. J.* 71 (2007) 1796–1806.
- [27] K.Y. Foo, B.H. Hameed, Insights into the modeling of adsorption isotherm systems, *Chem. Eng. J.* 156 (2010) 2–10.

- [28] T.W. Webber, R.K. Chakkravorti, Pore and solid diffusion models for fixed-bed adsorbers, *AIChE J.* 20 (1974) 228–238.
- [29] G. Crini, H.N. Peindy, F. Gumbert, C Robert, Removal of C.I. Basic Green 4 (Malachite Green) from aqueous solutions by adsorption using cyclodextrin-based adsorbent: Kinetic and equilibrium studies, *Sep. Purif. Technol.* 53 (2007) 97–110.
- [30] A. Dabrowski, Adsorption—From theory to practice, *Adv. Colloid Interface Sci.* 93 (2001) 135–224.
- [31] Y.S. Ho, J.F. Porter, G. McKay, Equilibrium isotherm studies for the sorption of divalent metal ions onto peat: Copper, nickel and lead single component systems, *Water Air Soil Pollut.* 141 (2002) 1–33.
- [32] Y. Kim, C. Kim, I. Choi, S. Rengraj, J. Yi, Arsenic removal using mesoporous alumina prepared via a templating method, *Environ. Sci. Technol.* 38 (2004) 924–931.
- [33] L.V. Radushkevich, Potential theory of sorption and structure of carbons, *Zh. Fiz. Khim.* 23 (1949) 1410–1420.
- [34] M.M. Dubinin, Modern state of the theory of volume filling of micropore adsorbents during adsorption of gases and steams on carbon adsorbents, *Zh. Fiz. Khim.* 39 (1965) 1305–1317.
- [35] A.S. Özcan, B. Erdem, A. Özcan, Adsorption of Acid Blue 193 from aqueous solutions onto BTMA-bentonite, *Colloids Surf. A: Physicochem. Eng. Asp.* 266 (2005) 73–81.
- [36] O. Redlich, D.L. Peterson, A useful adsorption isotherm, *J. Phys. Chem. A.* 63 (1959) 1024–1024.
- [37] K. Vasanth Kumar, S. Sivanesan, Comparison of linear and non-linear method in estimating the sorption isotherm parameters for safranin onto activated carbon, *J. Hazard. Mater.* 123 (2005) 288–292.
- [38] Y.S. Ho, Selection of optimum sorption isotherm, *Carbon.* 42 (2004) 2113–2130.
- [39] F.-C. Wu, R.-L. Tseng, R.-S. Juang, Adsorption of dyes and phenols from water on the activated carbons prepared from corncob wastes, *Environ. Technol.* 22 (2001) 205–213.
- [40] S. Lagergren, Zur theorie der sogenannten adsorption gelöster stoffe (For the theory of known adsorption of dissolved substances), *Kungliga Svenska Vetenskapsakademiens Handlingar* 24 (1898) 1–39.
- [41] Y.S. Ho, G. McKay, Pseudo-second order model for sorption processes, *Process Biochem.* 34 (1999) 451–465.
- [42] Y.S. Ho, Second-order kinetic model for the sorption of cadmium onto tree fern: A comparison of linear and non-linear methods, *Water Res.* 40 (2006) 119–125.
- [43] A. Taylor, N. Thon, Kinetics of chemisorption, *J. Am. Chem. Soc.* 74 (1952) 4169–4173.
- [44] Y.B. Zeldovich, Theoretical foundations of combustion processes, *Acta physicochim. U.R.S.S.* 1 (1934) 449–469.
- [45] S. Roginskii, Y.B. Zeldovich, On the theory of Freundlich adsorption isotherm, *Acta physicochim. U.R.S.S.*, 1 (1935) 961–974.
- [46] S.Y. Elovich, G.M. Zhabrova, Mechanism of catalytic hydrogenation of ethylene on nickel. 1. Kinetics of the process, *Zh. Fiz. Khim. (U.R.S.S.)* 13 (1939) 1761–1775.
- [47] W.J. Weber Jr, J.C. Morris, Intraparticle diffusion during the sorption of surfactants onto activated carbon, *J. Saint. Eng. Div. Am. Soc. Civil Eng.*, 89 (1963) 53–61.
- [48] Y. Yao, F. Xu, M. Chen, Z. Xu, Z. Zhu, Adsorption behavior of methylene blue on carbon nanotubes, *Bioresour. Technol.* 101 (2010) 3040–3046.
- [49] S. Hong, C. Wen, J. Hea, F. Gana, Y.-S. Ho, Adsorption thermodynamics of Methylene Blue onto bentonite, *J. Hazard. Mater.* 167 (2009) 630–633.
- [50] U. Farooq, J.A. Kozinski, M.A. Khan, M. Athar, Biosorption of heavy metal ions using wheat based biosorbents—A review, *Bioresour. Technol.* 101 (2010) 5043–5053.
- [51] M. Kara, H. Yuzer, E. Sabah, M.S. Celik, Adsorption of cobalt from aqueous solutions onto sepiolite, *Water Res.* 37 (2003) 224–232.
- [52] Yu Liu, Ya-Juan Liu, Biosorption isotherms, kinetics and thermodynamics, *Sep. Purif. Technol.* 61 (2008) 229–242.
- [53] Y.A. Aydın, N.D. Aksoy, Adsorption of chromium on chitosan: Optimization, kinetics and thermodynamics, *Chem. Eng. J.* 151 (2009) 188–194.
- [54] Y.S. Ho, G. McKay, Kinetic models for the sorption of dye from aqueous solution by wood, *Process Saf. Environ. Prot.* 76 (1998) 183–191.
- [55] O. Hamdaoui, Batch study of liquid-phase adsorption of methylene blue using cedar sawdust and crushed brick, *J. Hazard. Mater.* 135 (2006) 264–273.
- [56] M. Can, E. Bulut, A. Örneç, M. Özacar, Synthesis and characterization of valonea tannin resin and its interaction with palladium (II), rhodium (III) chloro complexes, *Chem. Eng. J.* 221 (2013) 146–158.
- [57] Y. Yao, F. Xu, M. Chen, Z. Xu, Z. Zhu, Adsorption behavior of methylene blue on carbon nanotubes, *Bioresour. Technol.* 101 (2010) 3040–3046.
- [58] G. McKay, M.S. Otterburn, J.A. Aga, Fuller's earth and fired clay as adsorbents for dyestuffs, *Water Air Soil Pollut.* 26 (1985) 149–161.
- [59] K. Porkodia, K. Vasanth, Kumar, equilibrium, kinetics and mechanism modeling and simulation of basic and acid dyes sorption onto jute fiber carbon: Eosin yellow, malachite green and crystal violet single component systems, *J. Hazard. Mater.* 143 (2007) 311–327.
- [60] I.A. Aguayo-Villarreal, L.A. Ramírez-Montoya, V. Hernández-Montoya, A. Bonilla-Petriciolet, M.A. Montes-Morán, E.M. Ramírez-López, Sorption mechanism of anionic dyes on pecan nut shells (*Carya illinoensis*) using batch and continuous systems, *Ind. Crops Prod.* 48 (2013) 89–97.
- [61] P.R. Bonelli, P.A. Della Rocca, E.G. Cerrella, A.L. Cukierman, Effect of pyrolysis temperature on composition, surface properties and thermal degradation rates of Brazil nut shells, *Bioresour. Technol.* 76 (2001) 15–22.
- [62] A. Demirbaş, Effect of temperature on pyrolysis products from four nut shells, *J. Anal. Appl. Pyrolysis* 76 (2006) 285–289.
- [63] H.M.F. Freundlich, Über die adsorption in lösungen (On the adsorption in solutions), *Z. Phys. Chem.* 57 (1906) 385–471.
- [64] M.I. Temkin, Adsorption equilibrium and kinetics of processes on heterogeneous surfaces and at interaction between adsorbed molecules, *Russian Journal of Physical Chemistry* 15 (1941) 296.